Performance Comparison of Fused Soft Control/Hard Observer Type Controller With Hard Control/Hard Observer Type Controller for Switched Reluctance Motors

Chunming Shi, *Member, IEEE,* and Adrian David Cheok, *Member, IEEE*

***Abstract*—Both soft computing (SC) and hard computing (HC) techniques are often successful for solving real-world control problems. In cases where problems could be solved by either or both methodologies, an important research problem is to find what are the advantages for fusing SC methods together with HC methods, rather than using the HC method alone. Hence, in this paper, a performance comparison is detailed for a fused soft control/hard observer type controller (where a classical or HC type observer is fused with an adaptive fuzzy or SC type controller) and a hard control/hard observer type controller (where both the observer and feedback linearization controller are classical HC types). The domain in which this comparison is made is for the sensorless speed control of switched reluctance motors (SRMs). This is because this type of motor has highly nonlinear characteristics, and the HC type controller can often be detrimentally affected by modeling inaccuracies, as well as noise.**

Simulation and experimental results are illustrated to show the performance comparison of the soft control/hard observer type controller and the hard control/hard observer type controller under a wide range of identical operation conditions including transient speed and torque, SRM model parameter variations, and measurement noise. It can be seen from the results that the soft control/hard observer type exhibits a better performance than the hard control/hard observer type controller.

***Index Terms*—Adaptive fuzzy control, feedback linearization, hard computing, observer, Lyapunov methods, soft computing.**

I. Introduction

SWITCHED reluctance motors (SRMs) can be applied in many industrial applications due to their cost advantages and ruggedness. However, the motor is highly nonlinear and operates in saturation to maximize the output torque. Moreover, the motor torque is a nonlinear function of current and rotor position. This highly coupled nonlinear and complex structure of the SRM makes it difficult to design a controller. Various control strategies have been proposed for control of SRM, such as feedback linearizing control [1], variable structure control [2], hybrid control [3], and adaptive fuzzy control [4].

Furthermore, in order to obtain high performance from an SRM, its stator windings must be excited in synchronism with the angular position of the rotor. Position sensors are commonly employed to obtain rotor position measurements, however, in many systems advantages can be found in eliminating these sensors. These benefits include the elimination of electrical connections to the sensors, reduced size, low maintenance, and insusceptibility to environmental factors. Hence a diverse range of indirect, or sensorless position estimation methods, has previously been proposed [5]–[8].

However, the prior research in sensorless control of SRM has two limitations.

- There have been few attempts to combine position and/or velocity estimation with advanced control to obtain a high performance sensorless control system [9].
- There has been scarce vigorous attempts to compare the performance among the hard computing type and soft computing type control strategies for this and similar applications.

Both soft computing (SC) and hard computing (HC) techniques are often successful for solving the SRM control problem. Hence, an important research question is what are the advantages for fusing SC methods together with HC methods, rather than using the HC methods alone. In particular HC type controllers can often be detrimentally affected by modeling inaccuracies and noise, and hence one should directly demonstrate the advantage of fusing soft and hard methods under these circumstances.

Thus, in this paper, two sensorless speed controllers for SRM have been proposed and compared: one is a fused soft control/hard observer type controller (SCHOC) (where a classical or HC type observer is fused with an adaptive fuzzy SC type controller), and the other is a hard control/hard observer type controller (HCHOC) (where both the observer and feedback linearization controller are classical HC types).

A nonlinear reduced order observer is used in both the HCHOC and the SCHOC to provide position and velocity estimations for the SRM. In the HCHOC, a feedback linearization controller with a robust term is adopted. In the SCHOC, instead of utilizing feedback linearization technique (which essentially demands a high-precision model parameters and accurate position and velocity information), a soft computing type adaptive fuzzy controller is proposed.

The adaptive fuzzy controller has the following three features.

- It uses fuzzy sets which have an ability to be robust to noise.

Manuscript received March 15, 2001; revised June 18, 2002.

The authors are with the Department of Electrical Engineering, National University of Singapore, Singapore 117576 (e-mail: adriancheok@nus.edu.sg).

Digital Object Identifier 10.1109/TSMCC.2002.801724.

- It uses adaptive fuzzy systems to replace the analytic functions derived from the SRM model. Hence it can reduce the sensitivity to modeling errors and noise.
- It deals with external disturbances and measurement noises by employing both a robust term and online tuning of the adaptive fuzzy systems.

The first feature arises from the width or size of the membership functions of the fuzzy sets in fuzzy systems. This width can be considered as an allowable level of noise [10], [11]. This means that an input data point with error or noise can still be placed in the same fuzzy set as the same input data with no error or noise. Thus, by fuzzification of the input signals, input data which is corrupted by noise can be accepted in the same set as the same data without noise but with a different membership function [12]. The length or range of the fuzzy set membership function will determine the range of values that will be accepted as part of the same set. The range can be defined such that small deviations or noise in the input data do not have a significant effect on the output position estimation.

However, it should also be noted that a disadvantage of using fuzzy rule based modeling is that an inverse relationship exists between *robustness* and *resolution*. As the robustness to input signal noise and error increases due to a widening of the fuzzy sets, the output resolution decreases due to the wider partitioning of the input and output signal domains. Therefore a balance must be found between error robustness and output resolution.

Thus, as it will be shown below, by the combination of the observer and adaptive fuzzy controller, the SCHOC provides a high performance speed controller for SRM and can reduce the sensitivity to modeling the highly nonlinear characteristics of SRM seen in hard-only methods. Furthermore, it provides satisfactory position and velocity estimations, and therefore overcomes the disadvantages of using sensors. Additionally, the scheme provides a high robustness to modeling errors, measurement noises and inaccurate position and velocity information, which is inevitable when the observer is converging.

The paper is organized as follows. First, the SRM model is described in Section II. The reduced order observer is introduced briefly in Section III. In Section IV, the HCHOC for SRMs with robustness consideration is presented. Then in Section V, the SCHOC for SRMs is formulated. In Section VI, simulation results are illustrated to show the performance comparisons between the SCHOC and the HCHOC under a wide range of identical operation conditions of SRM to confirm the advantages of the SCHOC. Finally, experimental results are shown in Section VII, and conclusions are given in Section VIII.

II. SRM Model

The principle of operation of SRMs is introduced here first, in order to derive the model used in this research later. A cross-sectioned picture of a four-phase SRM is shown in Fig. 1, where for clarity only one of the four phases winding has been drawn. The SRM consists of stators and rotors with salient poles. Each stator phase circuit is composes of two coils, wound around opposite stator poles. Due to the symmetry of the motor phases, the mutual inductance between the phases is negligible, and the rotor

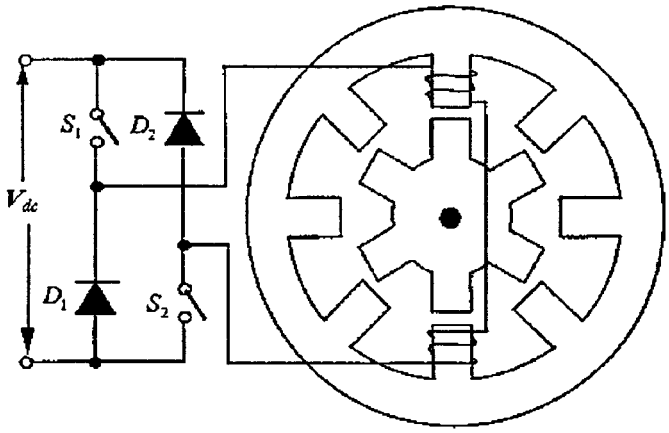

Fig. 1. Cross-sectional view of a four-phase SRM.

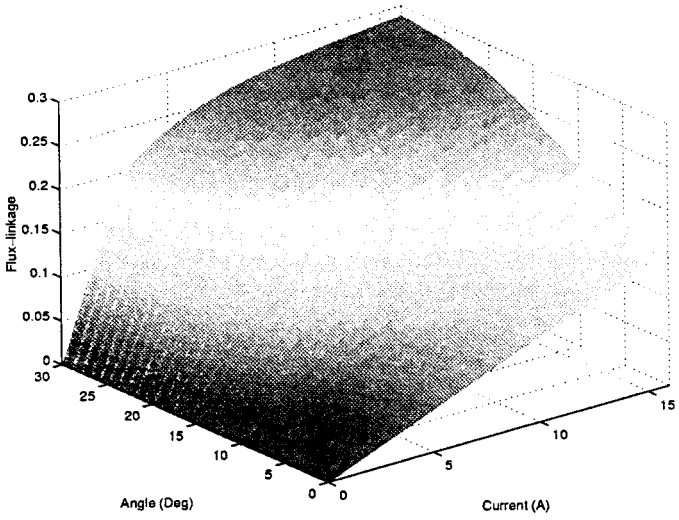

Fig. 2. Measured magnetic characteristics of an SRM.

position is detectable modulo $2\pi/N_r$, where N_r is the number of rotor poles.

The excitation of a phase produces a torque which causes the rotor to align, in a position of minimum reluctance with the poles of the driven phase circuit. A continuous rotation of the SRM can therefore be obtained by sequentially energizing the stator phases. It should be noted though that the excitation must be synchronous to the rotor position.

As mentioned above, the SRM has highly nonlinear characteristics and often operates in saturation to maximize the output torque. In Fig. 2, the highly nonlinear magnetic characteristics of an SRM can be seen in the relationship of the flux-linkage with rotor position and current. In the figure, zero degrees represents the unaligned rotor position and thirty degrees represents the aligned position.

In this work, an SRM model is needed to design the observer and controllers. The model suggested in [1] which takes magnetic saturation into account is adopted here. The general voltage equation of a q-phase SRM is given by

$$\frac{d\psi_j}{dt} = -ri_j + u_j \tag{1}$$

where u_j is the voltage across the stator terminals of the jth phase, r is the phase resistance, i_j is the current flowing in the jth phase, and ψ_j is the flux-linkage of the jth phase respectively.

The flux-linkage ψ_j is a nonlinear function of rotor position, due to the alignment between rotor and stator poles. It is also a nonlinear function of stator current i_j due to the magnetic saturation. Hence, the flux-linkage can be modeled [1] as

$$\psi_j(\theta, i_j) = \psi_s\left(1 - e^{-i_j f_j(\theta)}\right) \qquad i_j \geq 0 \tag{2}$$

where ψ_j is the saturation flux-linkage, and $f_j(\theta)$ can be represented by

$$f_j(\theta) = a + b\sin[N_r\theta - 2\pi j/q] \tag{3}$$

where a and b are suitable constants with $a > b$, N_r is the number of rotor poles, and $\theta = 0°$ and $\theta = 30°$ are the unaligned and aligned positions, respectively.

Using the coenergy function, the electromagnetic torque produced by jth phase can be given by [13]

$$T_j = \frac{\psi_s}{f_j^2}\frac{\partial f_j}{\partial \theta}\left[1 - (1 + i_j f_j)e^{-i_j f_j}\right]. \tag{4}$$

Finally, we give the motor model in order $(q+2)$ state space form. As a usual assumption, the load torque is assumed to be the combination of viscous friction of value B and an unknown one T_l

$$\dot{\theta} = \omega \tag{5}$$

$$\dot{\omega} = \alpha = \frac{1}{J}\left(\sum_{j=1}^{q} T_j - B\omega - T_l\right) \tag{6}$$

$$\dot{i}_j = \left(\frac{\partial \psi_j}{\partial i_j}\right)^{-1}\left(-ri_j + u_j - \frac{\partial \psi_j}{\partial \theta}\theta\right) \tag{7}$$

where ω is rotor velocity, and α is rotor acceleration. The nonlinear terms T_j , $\partial\psi_j/\partial i_j$ and $\partial\psi_j/\partial\theta$ are modeled according to equations (1)–(4).

III. Hard Computing Type Observer

To provide position and speed information for sensorless control of the SRM, a classical hard computing (or analytic model based) type observer introduced in [8] is adopted here. The observer is introduced by modeling the SRM dynamics and adding appropriate correction terms. Since q stator phase currents in SRM are easily measured without resorting to special sensors, they are suitable to design the correction terms. Hence, the position and velocity are the only two states to be estimated, which means a lower computational load and less complexity to design and analysis, especially when the SRM has many stator poles. Furthermore, we add a new state variable T_l for observer to estimate the external unknown load torque since controller itself has no means to obtain such information.

It is a reasonable and frequent assumption to let the unknown load torque be almost constant. This is because that, in practice, load variations are usually much slower than the electrical time constants. Thus we have

$$\dot{T}_l = 0. \tag{8}$$

The whole order three observer is presented in the following equations:

$$\dot{\hat{\theta}} = \hat{\omega} + g_1\varepsilon \tag{9}$$

$$\dot{\hat{\omega}} = \hat{\alpha} + g_2\varepsilon \tag{10}$$

$$\dot{\hat{T}}_l = g_3\varepsilon \tag{11}$$

$$\varepsilon = \sum_{j=1}^{q}\left(\dot{i}_j - \dot{\hat{i}}_j\right) \tag{12}$$

where g_1, g_2 and g_3 are observer gains to be designed and

$$\dot{\hat{i}}_j = \left(\frac{\partial \hat{\psi}_j}{\partial i_j}\right)^{-1}\left(-ri_j + u_j - \frac{\partial \hat{\psi}_j}{\partial \hat{\theta}}\hat{\omega}\right) \tag{13}$$

$$\hat{\psi}_j\left(\hat{\theta}, i_j\right) = \psi_s\left(1 - e^{-i_j f(\hat{\theta})}\right) \tag{14}$$

$$\hat{\alpha} = \frac{1}{J}\left(\sum_{j=1}^{q} T_j\left(\hat{\theta}\right), i_j - B\hat{\omega} - \hat{T}_l\right). \tag{15}$$

Note that acquirement of the order three observer (9)–(12) is independent of the specific form of the SRM model. In other words, any other forms of SRM model (such as the classic nonlinear SR model of [14]) could be adopted, as long as (12) is calculatable.

Then, the error dynamics can be obtained as the difference between (8)–(11) and (5) and (6). As has been demonstrated in [8], the observer gains g_1, g_2 and g_3 can be designed using Lyapunov technique so as to guarantee the observer's exponential convergence. Furthermore, the observer presents a very satisfactory performance in the whole speed range, and is robust to parameter variations and modeling errors.

IV. Hard Control–Hard Observer Type Controller (HCHOC)

As mentioned above, in this research the direct advantages of fusing soft computing with hard computing are investigated. Hence the first step is to derive a hard controller which uses classical feedback linearization [15]. To derive this controller we first differentiate (6) and get

$$\begin{aligned}\ddot{\omega} = {} & \frac{1}{J}\left[\sum_{j=1}^{q}\psi_j\frac{dR_j(\theta)}{d\theta}k_j\right]u(t) \\ & + \frac{1}{J}\left[r\sum_{j=1}^{q}\frac{1}{2}\psi_j\frac{dR_j(\theta)}{d\theta}i_j\right. \\ & \left. - \omega\sum_{j=1}^{q}\psi_j^2\frac{d^2R_j(\theta)}{d\theta^2} - B\frac{d\omega}{dt}\right] \\ = {} & f(X) + g(X)u(t)\end{aligned} \tag{16}$$

where $X = [i_1, i_2, i_3, i_4, \theta, \omega]^T$, $j = 1, 2, \ldots q$, and k_j is dictated by the electronic commutation signals and is defined as

$$k_j = \begin{cases} 1, & \text{when the } j\text{th phase should be on;} \\ -1, & \text{when the } j\text{th phase should be off and } i_j \neq 0; \\ 0, & \text{when the } j\text{th phase should be off and } i_j = 0. \end{cases} \tag{17}$$

Note that $g(X) = 0$ can be avoided because a two-phase-on scheme is adopted in this work [16], thus the dynamics (16) are controllable.

We define the tracking error as $e = \omega_r - \omega$, estimation error $\hat{e} = \omega_r - \hat{\omega}$, observation error $\tilde{e} = e - \hat{e}$, tracking error vector $E = [e, \dot{e}]^T$, and the estimation error vector $\hat{E} = [\hat{e}, \dot{\hat{e}}]$, where ω_r is the reference speed.

Since $f(X)$ and $g(X)$ are known functions derived from the SRM model, we can design control law using feedback linearization as form of

$$u = \frac{1}{g\left(\hat{X}\right)}\left[-f\left(\hat{X}\right) + \ddot{\omega}_r + K^T\hat{E} + R\right] \tag{18}$$

where $\hat{X} = [i_1, i_2, i_3, i_4, \hat{\theta}, \hat{\omega}]^T$, $K = (k_2, k_1)^T$ is feedback gain vector, and R is the robust term to be designed to compensate for disturbance.

Substituting (18) into (16), we can obtain the error dynamics

$$\ddot{e} = -K^T\hat{E} - R + f\left(\hat{X}\right) - f(X) + \left[g\left(\hat{X}\right) - g(X)\right]u. \tag{19}$$

Rewrite (19) and we can have

$$\dot{\hat{E}} = A\hat{E} + B[D_1 - R] \tag{20}$$

where

$$A = \begin{bmatrix} 0 & 1 \\ -k_2 & -k_1 \end{bmatrix}, \qquad B = \begin{bmatrix} 0 \\ 1 \end{bmatrix} \tag{21}$$

and D_1 is the disturbance term due to the observation error

$$D_1 = f\left(\hat{X}\right) - f(X) + \left[g\left(\hat{X}\right) - g(X)\right]u - \ddot{\tilde{e}}. \tag{22}$$

Note that D_1 is bounded because of observer's exponential convergence [8]. Thus, D_1 could be assumed to satisfy

$$||D_1|| \leq \rho \tag{23}$$

where ρ is a positive constant.

Now our objective is to design the robust term R using Lyapunov techniques to guarantee the overall stability of the sensorless control system. First, we define a Lyapunov function candidate

$$V\left(\hat{E}\right) = \tfrac{1}{2}\hat{E}^T P\hat{E} > 0 \tag{24}$$

where P is a positive definite matrix.

Differentiating (24) we can get

$$\dot{V}\left(\hat{E}\right) = \tfrac{1}{2}\hat{E}^T\left(A^TP + PA\right)\hat{E} + \hat{E}^TPB(D_1 - R). \tag{25}$$

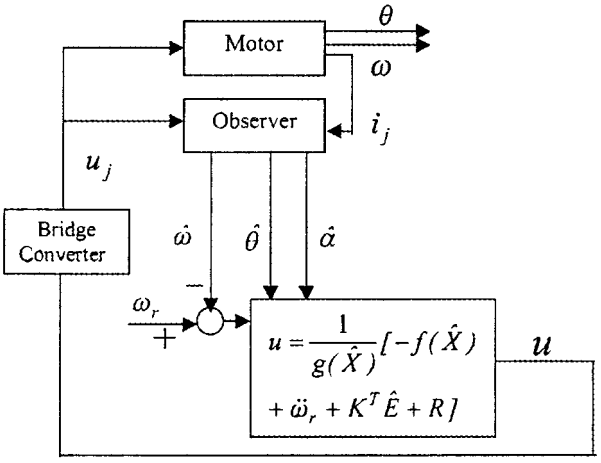

Fig. 3. Overall scheme of the HCHOC.

Since we can easily choose the feedback gain vector K to make A a stable matrix, the following Lyapunov equation stands

$$A^TP + PA = -Q \tag{26}$$

where Q is also a positive definite matrix.

Furthermore, we can choose the robust term R as

$$R = \rho * \operatorname{sgn}\left(\hat{E}^TPB\right). \tag{27}$$

Substituting (26) and (27) into (25), we have

$$\dot{V}\left(\hat{E}\right) \leq 0. \tag{28}$$

Thus, $V(\hat{E})$ is bounded because of (24) and (28). Furthermore, $\hat{E}$ is bounded hence both $\hat{e}$ and $\dot{\hat{e}}$ are bounded. Now we can have

$$\begin{aligned} \tfrac{1}{2}\lambda_{\min}(Q)\int_0^\infty \left\|\hat{E}\right\|^2 dt &\leq \int_0^\infty \hat{E}^TQ\hat{E}\,dt \\ &= V(0) - V(\infty) \leq V(0) \end{aligned} \tag{29}$$

where $\lambda_{\min}(Q)$ is the minimum eigenvalue for the matrix Q.

Equation (29) implies $\|\hat{E}\|$ is square integrable, thus $\hat{e}$ is square integrable. Note that $\dot{\hat{e}}$ is also bounded and thus $\lim_{t\to\infty}\hat{e}(t) = 0$. Note that $\lim_{t\to\infty}\tilde{e}(t) = 0$ and $e = \hat{e} + \tilde{e}$, hence $\lim_{t\to\infty}e(t) = 0$.

From the above deduction, we can see that if the control law is designed as (18) where the robust term R designed as (27), it is guaranteed that the control system is stable.

To summarize the above discussion, Fig. 3 shows the overall scheme of the HCHOC. It processes measured phase currents i_j as well as driving voltages u_j from the hard controller, and estimates the velocity $\hat{\omega}$ and position $\hat{\theta}$ of the rotor. The feedback linearization controller receives the estimated information and reference speed signal to calculate the driving voltages u_j.

Note that in this scheme, the phase voltages must be measured and known. This requires high-voltage sensors, with related isolation amplifiers and analog to digital converters. These circuits are normally expensive and require extra connections to the motor controller and drive. Thus, other methods which do not require the individual measurement of voltage can be used. For example, it is possible to calculate the phase voltages from

measuring the inverter dc link voltage only, together with knowledge of the PWM pulses [17]. This will be more beneficial and economical. However in this research, the main aim is to concentrate on two exact control schemes which differ in terms of being hard or soft. Thus, we use a simpler but more expensive phase voltage measurement scheme.

However, there are two problems associated with this HCHOC. First, ρ is difficult to obtain since there could be many possible factors contributing to the presence of D_1, such as SRM model parameter inaccuracies, or external noise. If ρ is not large enough, the overall stability cannot be guaranteed since it cannot fully compensate for the disturbance. On the other hand, too large a value of ρ is not desirable because it could cause the control saturation or chattering. Thus, problems can certainly arise when there are modeling inaccuracies and noise.

In addition, successful implementation of the HCHOC demands an accurate SRM model and position and velocity feedback. As we can see from (18), accurate control input $u(t)$ could be obtained only when $f(X)$ and $g(X)$ can be calculated accurately. Thus, once again, problems can arise in this method when there are modeling inaccuracies.

Hence, the above difficulties with using a hard type analytic model give an incentive to fuse soft computing techniques with this hard controller, and to directly compare their performance. This is to help overcome the demands for a high-precision model and accurate position and velocity information seen in the HCHOC scheme.

V. Fused Soft Control–Hard Observer Type Controller (SCHOC)

As mentioned above, there has been few vigorous attempt to compare the performance among the hard computing type and soft computing type control strategies for the SRM control and similar applications. However, an important research question is to determine and demonstrate the advantages for fusing SC methods together with HC methods, rather than using the HC method alone.

This is because, as mentioned above, the HC type controller can often only have a good performance if the model parameters are calculated correctly, and the noise is not high. Hence, in order to make a direct comparison, a fused soft control/hard observer type controller (SCHOC) is now defined.

Soft computing and fuzzy logic can be used to design nonlinear controllers, as is well justified by the Universal Approximation Theorem [18]. Furthermore, with adaptive fuzzy schemes, the controller can be made robust toward to plant model parameter variations and external bounded disturbance. Thus, a soft computing type adaptive fuzzy controller was adopted, as described in this section.

A. Description of Fuzzy System

Before proceeding with adaptive fuzzy controller design, a short description of fuzzy systems will be introduced first.

The basic configuration of fuzzy logic systems [19] consists of some fuzzy IF–THEN rules and a fuzzy inference engine. The fuzzy inference engine uses the fuzzy IF–THEN rules to perform a mapping from an input linguistic vector $X^T = [x_1 \;\; x_2 \;\; \cdots \;\; x_n]$ to an input linguistic variable $y \in R$. The ith fuzzy IF–THEN rule is written as

$$R^{(i)}\text{: if } x_1 \text{ is } A_1^i \text{ and } \cdots \text{ and } x_n \text{ is } A_n^i, \text{ then } y \text{ is } B^i \quad (30)$$

where A_1^i, A_2^i, $\ldots A_n^i$ are fuzzy sets.

By using product inference, center-average and singleton fuzzifier, the output of the fuzzy logic system can be expressed as

$$y(X) = \frac{\sum_{i=1}^{l} \overline{y}^i \left(\prod_{j=1}^{n} \mu_{A_j^i}(x_j) \right)}{\sum_{i=1}^{l} \left(\prod_{j=1}^{n} \mu_{A_j^i}(x_j) \right)} = W^T \phi(X) \quad (31)$$

where $\mu_{A_j^i}(x_j)$ is the membership function value of the fuzzy variable x_j, l is the number of the total IF–THEN rules, $\overline{y}^i$ is the point at which $\mu_{B^i}(\overline{y}^i) = 1$, $W^T = [\overline{y}^1, \overline{y}^2 \cdots \overline{y}^l]$ is the adjustable weight vector, $\phi^T = [\phi^1, \phi^2 \cdots \phi^l]$ is the fuzzy basis vector, and ϕ^i is defined as

$$\phi^i(X) = \frac{\left(\prod_{j=1}^{n} \mu_{A_j^i}(x_j) \right)}{\sum_{i=1}^{l} \left(\prod_{j=1}^{n} \mu_{A_j^i}(x_j) \right)}. \quad (32)$$

B. Adaptive Fuzzy Controller Design

To overcome the problems associated with the HCHOC discussed in the Section IV, instead of using $f(X)$ and $g(X)$ directly, we use two adaptive fuzzy systems $\hat{f}(\hat{X}|W_f)$ and $\hat{g}(\hat{X}|W_g)$ in the form of (31) here.

According to SRM dynamics (16), based on the Certainty Equivalence Approach [20], the control law can be designed as the form

$$u = \frac{1}{\hat{g}\left(\hat{X}\middle| W_g\right)} \left[-\hat{f}\left(\hat{X}\middle| W_f\right) + \ddot{\omega}_r + K^T \hat{E} + R \right] \quad (33)$$

where W_f and W_g are the adjustable weight vectors, and K and R share the same definitions in Section V-A.

Substituting (33) into (16), the error dynamics can be written as

$$\ddot{e} = -K^T \hat{E} - R + \hat{f}\left(\hat{X}\middle| W_f\right) - f(X) + \left[\hat{g}\left(\hat{X}\middle| W_g\right) - g(X)\right] u. \quad (34)$$

Rewrite (34) and we have

$$\dot{\hat{E}} = A\hat{E} + B\left[\tilde{W}_f^T \phi\left(\hat{X}\right) + \tilde{W}_g^T \phi\left(\hat{X}\right) u + D_1 + D_2 - R\right] \quad (35)$$

where $\tilde{W}_f = W_f - W_f^*$, $\tilde{W}_g = W_g - W_g^*$, W_f^* and W_g^* are the optimal weight vectors which lie in some convex regions [21],

D_1 is the same as in Section IV, D_2 is the disturbance term due to minimum approximation error

$$D_2 = f(X|W_f^*) - f(X) + [g(X|W_g^*) - g(X)]u. \quad (36)$$

For purpose of comparison of the two algorithms, first we adopt the same robustness term R as (27). Now our objective is to design adaptive laws for the two adaptive fuzzy systems $\hat{f}(\hat{X}|W_f)$ and $\hat{g}(\hat{X}|W_g)$. To achieve this goal, we define a Lyapunov function candidate

$$V\left(\hat{E}\right) = \frac{1}{2}\hat{E}^T P\hat{E} + \frac{1}{2\gamma_1}\tilde{W}_f^T\tilde{W}_f + \frac{1}{2\gamma_2}\tilde{W}_g^T\tilde{W}_g > 0 \quad (37)$$

where γ_1 and γ_2 are positive constants.

Differentiating equation (37) with respect to time gives

$$\begin{aligned}\dot{V}\left(\hat{E}\right) = {} & \tfrac{1}{2}\hat{E}^T\left(A^TP + PA\right)\hat{E} + \hat{E}^TPB(R - D_1 - D_2) \\ & + \frac{1}{\gamma_1}\tilde{W}_f^T\left(\dot{W}_f + \gamma_1\hat{E}^TPB\phi\left(\hat{X}\right)\right) \\ & + \frac{1}{\gamma_2}\tilde{W}_g^T\left(\dot{W}_g + \gamma_2\hat{E}^TPB\phi\left(\hat{X}\right)u\right). \quad (38)\end{aligned}$$

Now we choose the adaptive laws as

$$\dot{W}_f = -\gamma_1\hat{E}^TPB\phi\left(\hat{X}\right) \quad (39)$$

$$\dot{W}_g = -\gamma_2\hat{E}^TPB\phi\left(\hat{X}\right)u. \quad (40)$$

Substituting (27) and (39) into (38), we can obtain

$$\dot{V}\left(\hat{E}\right) = -\tfrac{1}{2}\hat{E}^TQ\hat{E} + \hat{E}^TPBD_2. \quad (41)$$

Based on the Universal Approximation Theorem [18], we can expect that the minimum approximation error D_2 should be small enough so that

$$\dot{V}(\bar{e}) \le 0. \quad (42)$$

Using the same procedures described in Section V-A, we can approve $\lim_{t\to\infty} e(t) = 0$.

However, adaptive laws (39) and (40) themselves cannot guarantee the convergences of W_f and W_g. To solve this potential problem, parameter projection algorithm can be used to modify the adaptive laws such that W_f and W_g will remain inside their constrain sets respectively [21], which are specified by the designer.

To summarize the above discussion, Fig. 4 shows the overall scheme of the SCHOC proposed in this paper. It processes measured phase currents i_j and driving voltages u_j from the hard controller and estimates the velocity $\hat{\omega}$ and position $\hat{\theta}$ of the rotor. The adaptive fuzzy SCHOC controller receives the estimated information and reference speed signal to calculate the driving voltages and adjust the parameters of the fuzzy system online using the adaptive laws (39).

As the SCHOC fuses both soft computing methods (fuzzy logic) and hard computing methods (mathematical observer), it can help overcome the disadvantages of sensitivity to inaccurate modeling and noise that can arise in the hard-only method. As

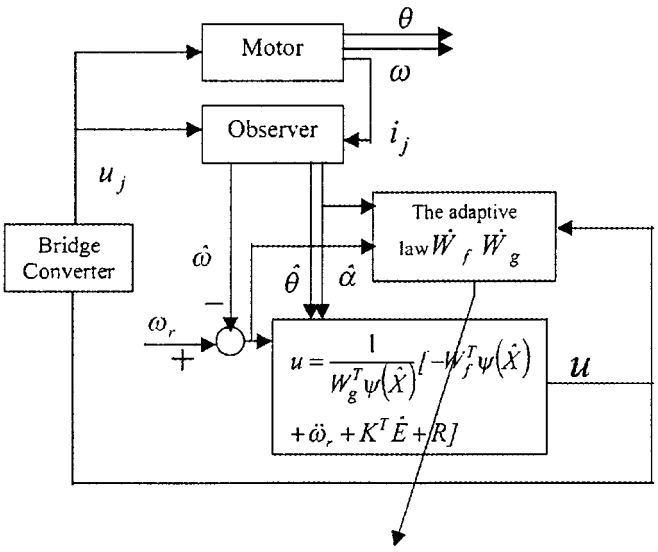

Fig. 4. Overall scheme of the SCHOC.

discussed above the hard-only method requires a high-precision model and accurate position and velocity information. Hence it is sensitive to noise and modeling errors.

Moreover, it is interesting to compare between the computational loads of the SCHOC and the HCHOC, which should be taken into account for practical implementation. As can be seen from equation (16), the model-based calculation of functions $f(X)$ and $g(X)$ is rather complex. Meanwhile, the computational load of functions of $\hat{f}(\hat{X})$ and $\hat{g}(\hat{X})$ is much lower due to the employment of the fuzzy rules. However, its overall computational load is increased due to the need to calculate the adaptive laws in equations (39) and (40). Thus, it could be concluded that the computational load of the SCHOC is higher than that of the HCHOC. In the experimental results that are shown below, it was found for the particular system, using exactly the same microprocessor and hardware, the sampling frequency could be set to a maximum of 8.7 kHz for the SCHOC and 10.8 kHZ for the HCHOC.

VI. Simulation Results

In the above discussion, two types of high performance sensorless SRM control methods were detailed, namely the hard-only HCHOC and the fused soft–hard SCHOC. Both of them combine position and velocity estimation with advanced control. However, one uses classical control methods exclusively whereas the other applies soft computing/fuzzy logic together with the hard computing methodology. One of aim of this research is to throughout compare the two control techniques under identical operating conditions.

Thus, in this section, we will illustrate the performance comparisons of the SCHOC and the HCHOC under a wide range of identical operation conditions by MATLAB simulations. For purpose of fair comparison, all the common parts of the two sensorless controllers are set to be exactly the same.

The motor employed in these simulations has eight stator and six rotor poles with a step angle of 15°. Its parameter values are listed in the Appendix.

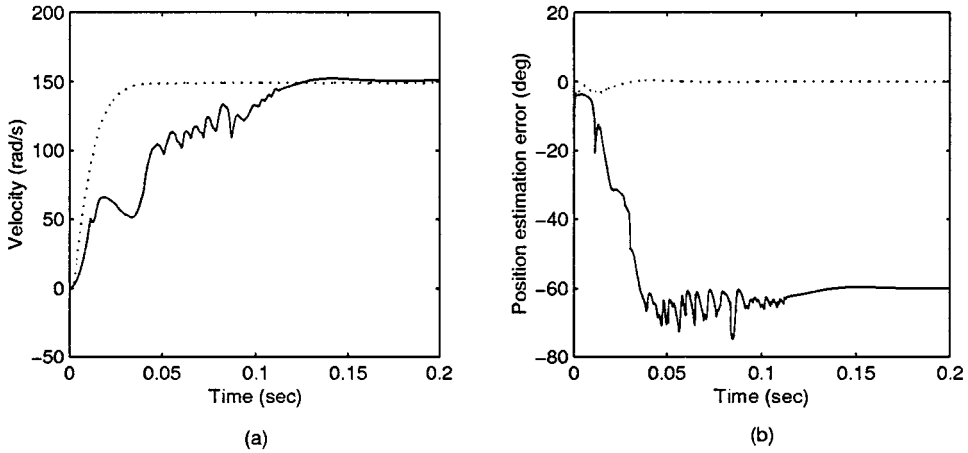

Fig. 5. (a) Actual speed responses and (b) position estimation errors of the SCHOC (dotted line) and the HCHOC (solid line) under initial position error 10°, $\omega_{ref} = 150$ rad/s.

The design parameters are selected as $g_1 = -0.01$, $g_2 = -0.20$, $g_3 = 0.015$, $Q = I_{2\times 2}$, $\rho = 10^3$, $\gamma_1 = 1(10^6)$, $\gamma_2 = 1(10^3)$, $k_1 = 340$, $k_2 = 4(10^4)$. The sampling frequency is 10 KHz.

In our research, the design parameters $g_1 = -0.01$, $g_2 = -0.20$ and $g_3 = 0.015$ are selected so as to guarantee the observer's exponential convergence [8]. Furthermore, the selections of ρ, γ_1 and γ_2 are based on the very rough ranges of functions $\hat{f}(\hat{X})$, $\hat{g}(\hat{X})$, $f(X)$ and $g(X)$, which can be derived from the SRM model parameters and simulations. This is justified by the fact that if these parameters are selected appropriately, the adaptive fuzzy systems could approximate the functions obtained from the model in a shorter time. Meanwhile, note that only very rough ranges (for example, in the same powers of ten of order), are needed to be known, due to the use of the adaptive laws. Thus, a very rough initial estimate is adequate.

For simplicity, in each of the two fuzzy systems, we only use the estimation velocity error $\hat{e}$ and acceleration error $\dot{\hat{e}}$ as the inputs, each with seven fuzzy sets on their ranges respectively. Because the number of states are two, the total numbers of fuzzy rules are 49. The initial values of adjustable weights are selected as

$$W_{f_i} = -1(10^6), \quad W_{g_i} = -2(10^4), \qquad i = 1, 2 \cdots 49. \tag{43}$$

Using the algorithms developed in Sections IV and V, the performances of both types of controllers have been simulated for a wide range of identical operating conditions. The results of these tests will be detailed below. Specifically, the robustnesses of both the HCHOC and the SCHOC toward parameter variations, external disturbance, and measurement noise will be examined and compared.

A. Startup

Successful startup of the SRM could be affected by many factors. Given a noise free environment and accurate SRM model parameters, startup of the SRM will be still affected by the initial position error between the actual rotor position and initial position used in the observer. For sensorless control system for SRM, initial position error is inevitable since sensorless algorithms always need time to converge. Thus in this test, the robustness against the initial position error is shown, while the robustness test to external noise will be examined later. The speed command in this test is set as 150 rad/s.

Fig. 5 shows the speed responses and position estimation errors of the HCHOC and the SCHOC when the SRM is started with an initial position error 10°, or 16% of one electrical cycle. It can be seen that for the SCHOC, it takes only about 0.05 s for the actual speed and position estimation error to converge, while for the HCHOC, it temporarily loses synchronism and reaches a new synchronism position of $-60°$ in about 0.15 s. Note that $-60°$ is equal to 0° due to the electrical cycle of 60° deriving from the structure symmetry of the four-phase SRM (which has an electrical cycle of four times 15°). Furthermore, the transient response of the SCHOC is much more smoother than the HCHOC. This is well justified by the fact that the HCHOC, as a fully model-based controller, also demands accurate position and velocity information in order to gain a high performance. However, for this sensorless system, the position and velocity information from the observer in transient period is not accurate when the observer is converging.

Hence, in this test, it is clearly shown that comparing with the HCHOC, the SCHOC is much more robust to initial position error, which is very important for a sensorless controller.

B. Step Changes in Reference Speed

In this test, the motor is started from zero speed with a speed command of 100 rad/s. The initial position error is set as 5°. The speed command changes to 200 rad/s at $t = 0.2$ s and 150 rad/s at $t = 0.4$ s.

Fig. 6 shows the actual speed responses and position estimation errors of the SCHOC and the HCHOC under these step changes in speed command. For clarity, its expanded view is shown in Fig. 7. We can see that in steady state, the SCHOC exhibits no noticeable steady state error and speed ripples, whereas for the HCHOC, both steady state error and speed ripples exist.

Furthermore, the SCHOC has demonstrated a much better transient state response than HCHOC after a change in the reference speed. This is despite a similar performance of position estimation in both the SCHOC and the HCHOC.

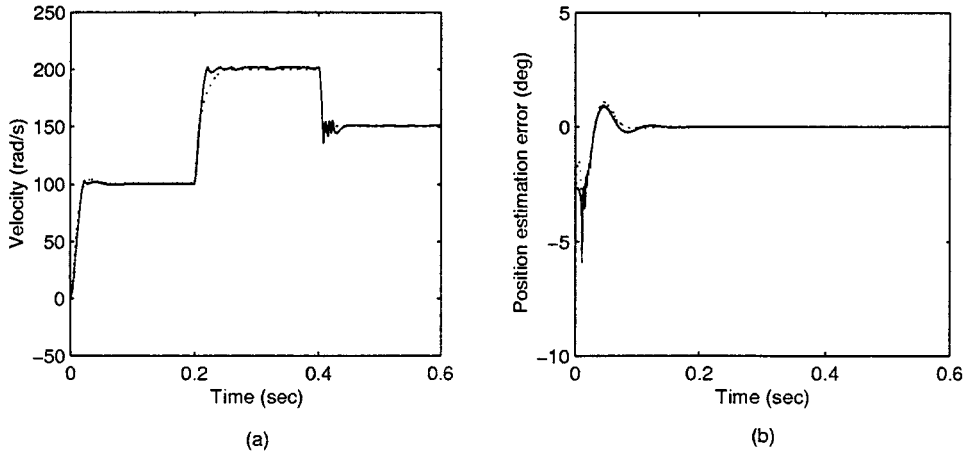

Fig. 6. (a) Actual speed responses and (b) position estimation errors of the SCHOC (dotted line) and the HCHOC (solid line) under step changes in ω_{ref}: 100 rad/s (0–0.2 s), 200 rad/s (0.2–0.4 s), 150 rad/s (0.4–0.6 s).

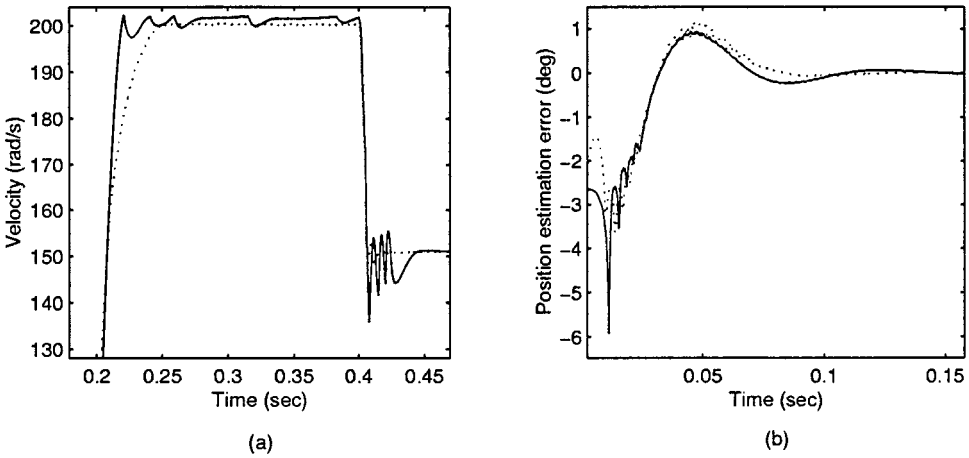

Fig. 7. Expanded view of (a) actual speed responses and (b) position estimation errors of the SCHOC (dotted line) and the HCHOC (solid line) under step changes in ω_{ref}: 100 rad/s (0–0.2 s), 200 rad/s (0.2–0.4 s), 150 rad/s (0.4–0.6 s).

Therefore the results above have shown that comparing with the HCHOC, the SCHOC can track variable reference speed more rapidly and smoothly without noticeable steady state error and speed ripples.

C. Unknown Load Torque

It is common that in many cases the SRM may be operated with an unknown load torque T_l. Thus, the performance comparison of the SCHOC and the HCHOC under unknown load torque is examined here. In this test, the external load torque is set to 0.4 Nm during the period 0–0.3 s, 0.1 Nm during the period 0.3–0.6 s, and 0.7 Nm during the period 0.6–1.0 s. The reference speed ω_{ref} is 150 rad/s and the initial estimated load torque is set as 0 Nm.

The unknown load torque and its estimates from the SCHOC and the HCHOC are shown in Fig. 8. Note that this is an extreme assumption regarding the load torque variation because the rate of load torque variations are usually much smaller in practice. From Fig. 8, we can see that the HCHOC exhibits a very large overshoot in load torque estimation, which will deteriorate the speed response accordingly. However, the SCHOC has a much smaller overshoot and settling time for the same condition.

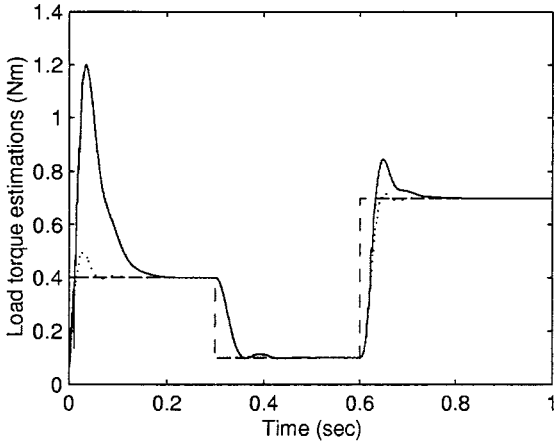

Fig. 8. Load torque estimation by the HCHOC (solid line) and by the SCHOC (dotted line) under step changes in T_l (dashed line): 0.4 Nm (0–0.3 s), 0.1 Nm (0.3–0.6 s), 0.7 Nm (0.6–1.0 s), $\omega_{ref} = 150$ rad/s.

Fig. 9 shows the speed responses and position estimations of the SCHOC and the HCHOC under these large step changes in the load torque. During the period 0–0.3 s, we can clearly see the overshoot in both speed response and position estimation error

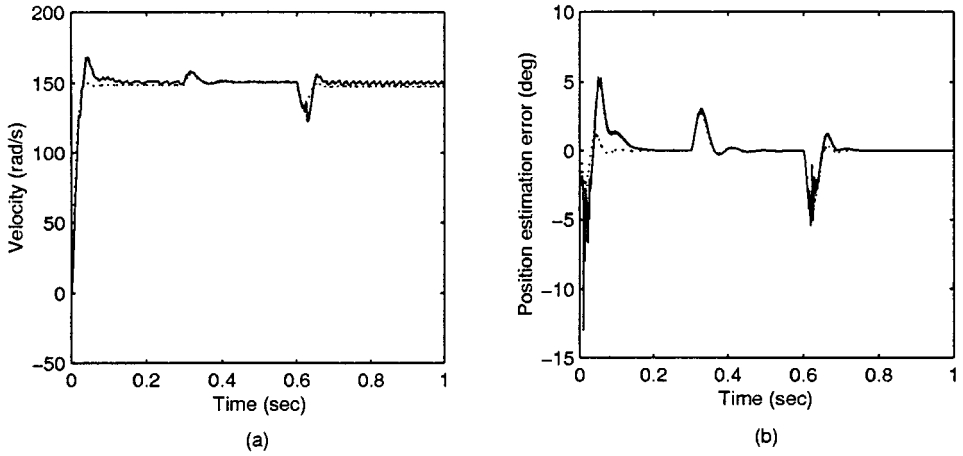

Fig. 9. (a) Actual speed responses; (b) position estimation errors of the HCHOC (solid line) and the SCHOC (dotted line) under step changes in T_l: 0.4 Nm (0–0.3 s), 0.1 Nm (0.3–0.6 s), 0.7 Nm (0.6–1.0 s), $\omega_{ref} = 150$ rad/s.

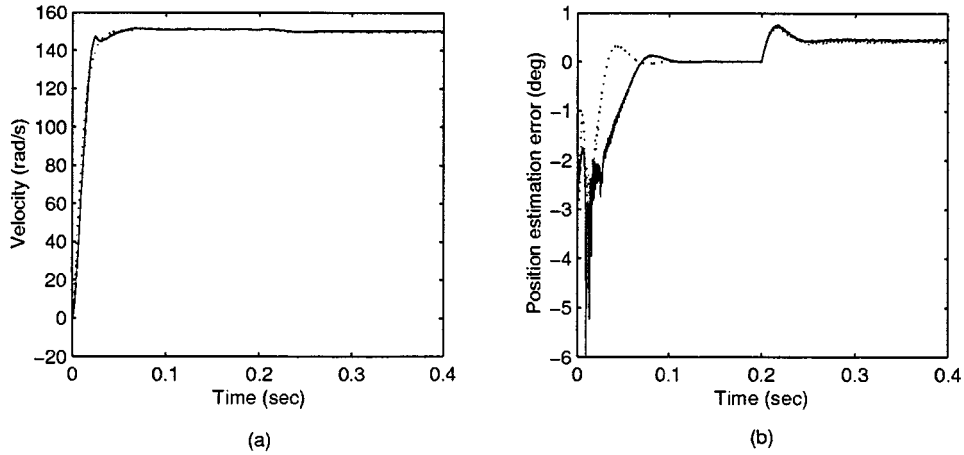

Fig. 10. (a) Actual speed responses; (b) position estimation errors of the HCHOC (solid line) and the SCHOC (dotted line) under model parameter variations: $r = 1.4\ \Omega$ (0–0.2 s), $r = 2.1\ \Omega$ (0.2–0.4 s), $\omega_{ref} = 150$ rad/s.

for the HCHOC, whereas the SCHOC presents a much smoother response. In addition, during the period 0.6–1.0 s, it can be seen that speed ripples still exists for the HCHOC even after the load torque estimation has converged.

Hence, the results above have shown a higher robustness of the SCHOC compared to the HCHOC with variable load torque. Comparing with the HCHOC, the advantages of the SCHOC for a step change in load torque include much less speed ripple in the steady state, a much smoother transient response, and faster convergence of load torque estimation and position estimation errors.

D. Parameter Variations

In this test the robustness of the SCHOC and the HCHOC toward parameter variations is examined. We distinguish between mechanical parameters (J, B) and electrical parameters. The mechanical parameters (J, B) can not always be obtained accurately and they may also vary during the SRM operation. However, the uncertainties on the mechanical parameters can be well handled by the process of load torque estimation. The reason is that the observer can estimate their effects as these are equivalent to load torque variations. Thus, in this section, only the test under electrical parameter variations is done here.

We illustrate the robustness toward electrical parameters by using stator phase resistance r as an example. During an SRM operation, r can increase due to temperature rise. At the beginning of this test, the measured $r = 1.4\ \Omega$ and r changes to $r = 2.1\ \Omega$ when $t = 0.2$ s. The speed command is 150 rad/s.

The results of Fig. 10 show quite similar performance of the SCHOC and the HCHOC against this resistance variation. For position estimation errors, we can see that there is a steady state error for both the SCHOC and the HCHOC.

However, it is acceptable that the steady state error is below 1°, or 1.5% of an electrical cycle when the stator phase resistance r varies its initial value by 50%. The reason is that in practice, the resistance will only vary slowly due to temperature changes.

Hence in this test, we demonstrated that both the SCHOC and the HCHOC are robust to the electrical parameter variations. Meanwhile, the mechanical parameter variations can be well handled by the observer as if they were due to load torque variations. This fact has been shown in Section VI-C.

E. Measurement Noise

Another very important aspect of robustness in the comparison of the soft computing type and classical type controllers is the robustness toward noise. In practice, motor drives are elec-

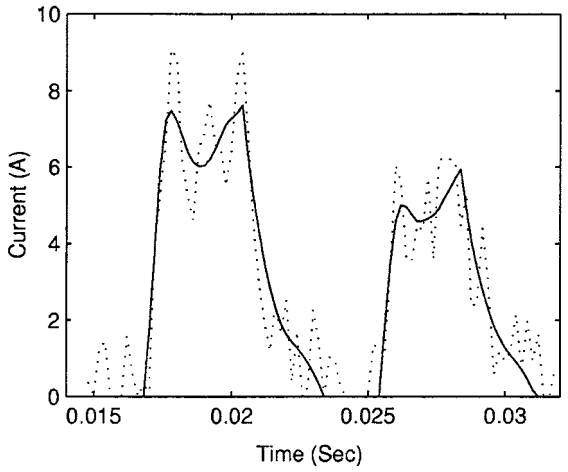

Fig. 11. Expanded comparison of current waveforms of one test: with (dotted line) and without noise (solid line), $\omega_{ref} = 150$ rad/s.

tromagnetically noisy environments, and in addition, measurement circuits of electronic signals are imperfect.

In this work, the measurements of voltages were relatively unaffected by noise for the following reasons. A high voltage constant dc supply was used, which contained a high level of capacitance across the dc bus. Thus, electromagnetic noise would not affect the high voltage amplitude with great significance, and the high capacitance ensured a filtering of any rapid changes of voltage arising from the supply of the motor phase currents. In addition, the voltage fed to the motor phases is a pulse width modulated form of the dc voltage, and thus it is a binary type signal (having either a high voltage dc value, or zero), and thus software or hardware filters can be fairly easily employed.

However the phase current can be critically affected by noise as it is a highly nonlinear waveform (and thus difficult to filter), and can have a low or high amplitude according to the exact phase condition. Thus, the measured currents will usually be corrupted by noise and error.

Furthermore, error will be introduced into the flux-linkage due to the integration process of (1). This will result in error in the estimated position because of the relationship of position with flux-linkage and current through magnetic characteristics $(\psi(\theta, i))$ of the SRM. The quantitative analysis of the effect of simultaneous errors in both the flux-linkage and current on position estimation has been detailed in [22].

To compare the robustness of the SCHOC and the HCHOC toward noise, firstly a very high noise with an amplitude of 20% of the maximum level of the measured current is added as an example. Note that in this test the motor is also started under external noise.

The added noise is Gaussian in nature, and therefore, has a finite variance. The expanded view of a typical current in Fig. 11 clearly shows that the current with noise deviates significantly at various points in time from the current without added noise. In this test, the speed command is 150 rad/s.

The speed response and the position estimation error of the SCHOC for one test are shown in Fig. 12. Thus we can clearly see the high robustness of the SCHOC. However, as we found out, the HCHOC fails to work under 20% noise in current measurement.

For comprehensive and fair comparisons, we have done ten tests for both the SCHOC and the HCHOC under added random Gaussian noises with an amplitude of 5%, 10%, and 20% of the maximum level of the measured current, respectively. A summary of the robustness tests toward noise is presented in Tables I–III, which give the average position estimation errors, maximum position estimation errors, average speed errors, and maximum speed errors of the ten tests.

The results of Tables I and II show when the amplitude of the added noises are relatively low, both the SCHOC and the HCHOC can work well. However, the advantage of the SCHOC can still be seen from the performance improvements. For a high current noise such as 20%, the SCHOC consistently shows its robustness whereas the HCHOC fails to work under these conditions.

Thus we can see that the HCHOC has a limited capacity to deal with the measurement noise in current. However, by adopting adaptive fuzzy systems, the SCHOC has shown more robustness toward external noise.

F. Standstill and Stall

One of the harshest tests of sensorless motor drive control is operation under a sudden stall. Thus, in this section, the performances of the SCHOC and the HCHOC when the SRM comes into a sudden stall are demonstrated. Actually, it can be treated as a special case when the SRM operates under variable load torque in that a very large unknown load torque is applied suddenly. In this test, the speed command ω_{ref} is 150 rad/s. A very large load torque for the SRM is suddenly applied at $t = 0.2$ s, which causes a standstill to the SRM.

Fig. 13 shows the performances under this situation. It can be seen that when SRM suddenly comes across a stall, the speed of both the HCHOC and the SCHOC will drop to around zero immediately. While the position estimation error from the HCHOC fails to converge, the SCHOC temporarily loses synchronism and reaches a new synchronism position of $-60°$ in about 0.6 s. Note that $-60°$ is in fact the same angle as $0°$, thus the position estimation error converges to approximate zero. Thus, it is shown the SCHOC can estimate the rotor position even when the SRM comes across a sudden standstill, which is a demonstration of the higher robustness of the SCHOC comparing with the HCHOC.

VII. Experimental Results

The actual operating effects of the SRM drive includes measurement error, noise, calculation error, non ideal devices, electromagnetic coupling, controller delays, quantization error, mutual inductance between motor phases, parameter variation of motor inductances and resistances, asymmetrical inductance variation in the motor phases, variation in the magnetization curves in each of the phases, and effects on the motor waveforms of eddy currents (which can distort the phase current, especially during current transients). Therefore, experimental waveforms should be used to verify the ability of the sensorless scheme to operate with a real SRM, as the above effects will affect the position estimation and prediction accuracy.

To obtain experimental results, an SRM drive system was designed and constructed with a controller. The drive consists

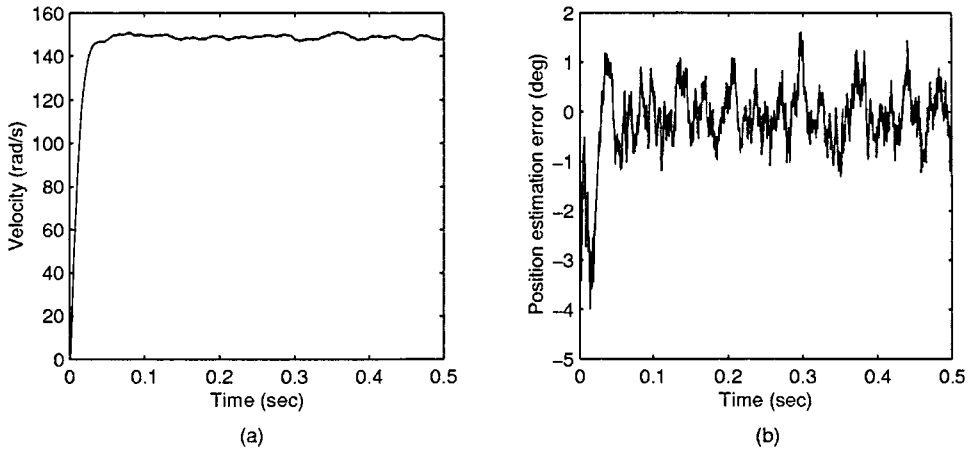

Fig. 12. (a) Actual speed response; (b) position estimation error of one test of the SCHOC when 20% of maximum amplitude noise in current is added, $\omega_{ref} = 150$ rad/s.

TABLE I
ROBUSTNESS TESTS AGAINST 5% NOISE IN CURRENT MEASUREMENT

	Average position estimation error	Maximum position estimation error	Average speed error	Maximum speed error
HCHOC	0.15°	1.39°	1.07 rad/s	2.11 rad/s
SCHOC	0.13°	0.60°	0.60 rad/s	1.60 rad/s
Improvement	13%	56%	44%	24%

TABLE II
ROBUSTNESS TESTS AGAINST 10% NOISE IN CURRENT MEASUREMENT

	Average position estimation error	Maximum position estimation error	Average speed error	Maximum speed error
HCHOC	0.31°	1.54°	1.08 rad/s	3.07 rad/s
SCHOC	0.26°	1.05°	0.85 rad/s	2.59 rad/s
Improvement	16%	32%	21%	16%

TABLE III
ROBUSTNESS TESTS AGAINST 20% NOISE IN CURRENT MEASUREMENT

	Average position estimation error	Maximum position estimation error	Average speed error	Maximum speed error
HCHOC	*fails*	*fails*	*fails*	*fails*
SCHOC	0.52°	2.03°	1.35 rad/s	4.36 rad/s

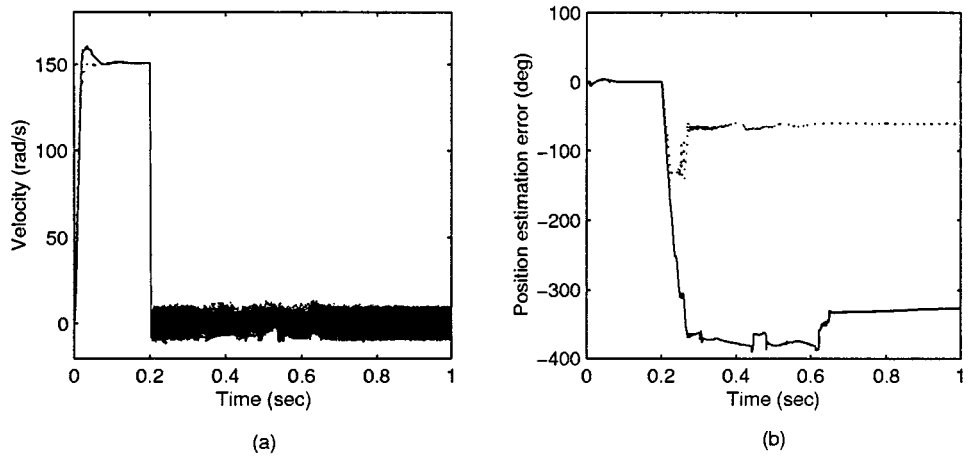

Fig. 13. (a) Actual speed responses; (b) position estimation errors of the HCHOC (solid line) and the SCHOC (dotted line) under standstill from $t = 0.2$ s, $\omega_{ref} = 150$ rad/s.

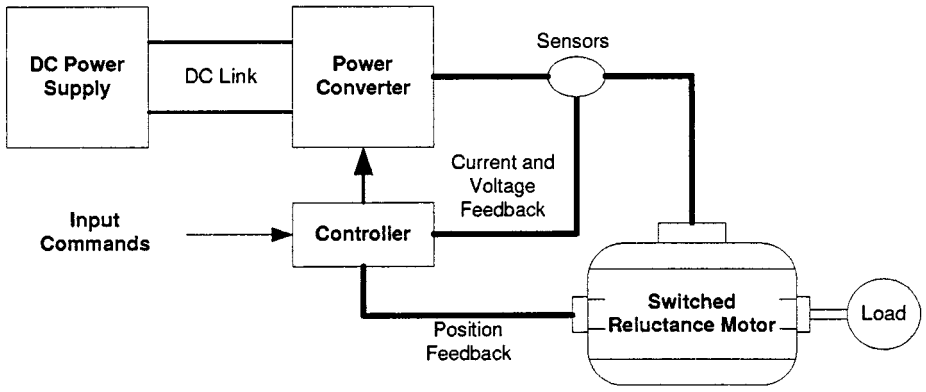

Fig. 14. Experimental system block diagram.

of several distinct subsystems: four-phase IGBT inverter (two switch per phase type), a dsp board (dSPACE 1003/1004 alpha combo DSP board), which performs data acquisition as well as real time data processing, a DS2201 Multi-I/O board which provides an interface between the DSP board and the measurement sensors. The current was measured with a hall effect current transducer which was based on the principle of magnetic compensation. The voltage was measured using isolated voltage sensors. Both the current sensor and the voltage sensor provide electronic measurement with galvanic isolation between the primary and the secondary circuits. A 12 bit absolute encoder was used to measure the rotor position. A regulated dc power supply, which can supply up to 20 A dc current, is used to energize the phase winding of SRM. The SRM tested by the measurement system was the same as that in the simulations. Fig. 14 shows the block diagram of the system setup, and Fig. 15 shows pictures of the laboratory setup as well as a close up of the motor system used for the experiment.

A. Startup and Transient Speed/Load Operation

In this test the motor is initially started with a mechanical load of 0.5 Nm and a reference speed of 100 rad/s. At time $t = 0.8$ s the speed command is step changed to 130 rad/s. Then at time $t = 1.5$ s, the load torque is doubled to 1.0 Nm. The test results can be seen in Fig. 16.

The conditions of this test allow the control methods to be experimentally tested for a number of important conditions. This includes start-up speed operation, change in speed command, and change in load torque.

The actual software was developed using Matlab, which is then converted to real time dsp code using the dSPACE system. Thus, due to this technique, it is not possible to predict the exact execution time of the algorithms (developed in Matlab) until the actual code running on the dsp is executed (although we aimed for 10 kHz because this was used for the simulation frequency). Hence it was found that in this system, using exactly the same microprocessor and hardware, the sampling frequency could be set to a maximum of 8.7 kHz for the SCHOC and 10.8 kHz for the HCHOC.

In the experimental tests, it was seen that similar to the simulation results that the SCHOC has a much faster response and settling time than the HCHOC. However, it was found that in

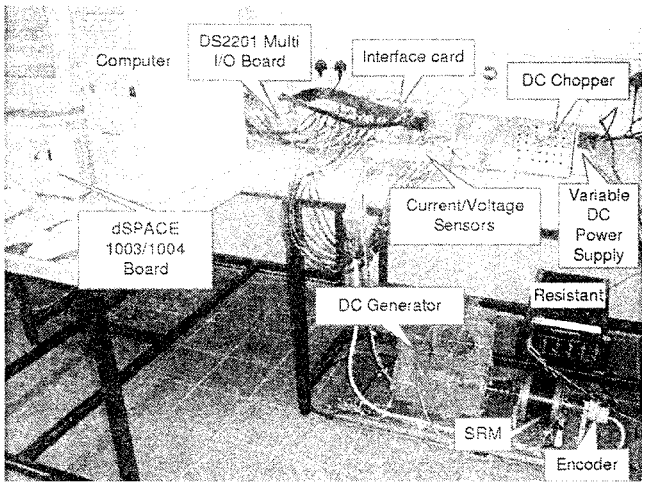

(a)

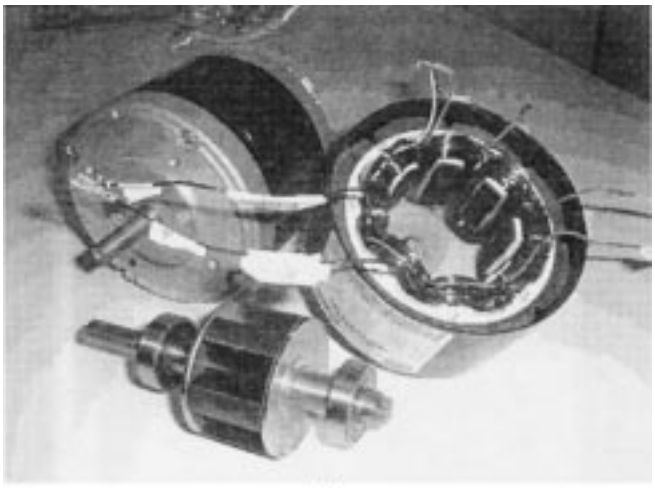

(b)

Fig. 15. Laboratory system photographs: (a) Complete system setup [note that the encoder is only used for measurement purposes and not control, and the dc generator is used for active loading (a separate torque transducer is not shown)] and (b) switched reluctance motor used in the experiment.

the experimental results that the transient over-shoot after start up was not acceptable for the SCHOC. Thus the results are not as ideal as the simulation results. The poorer performance in the experimental results can be explained by the fact that the actual

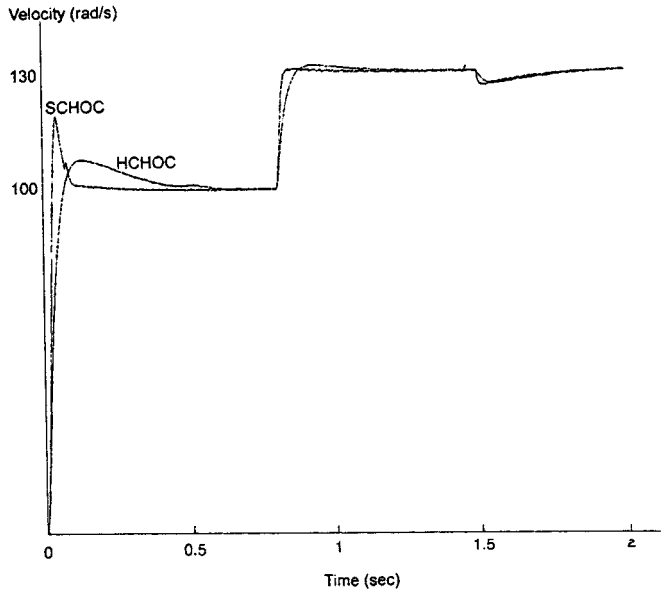

Fig. 16. Experimental results.

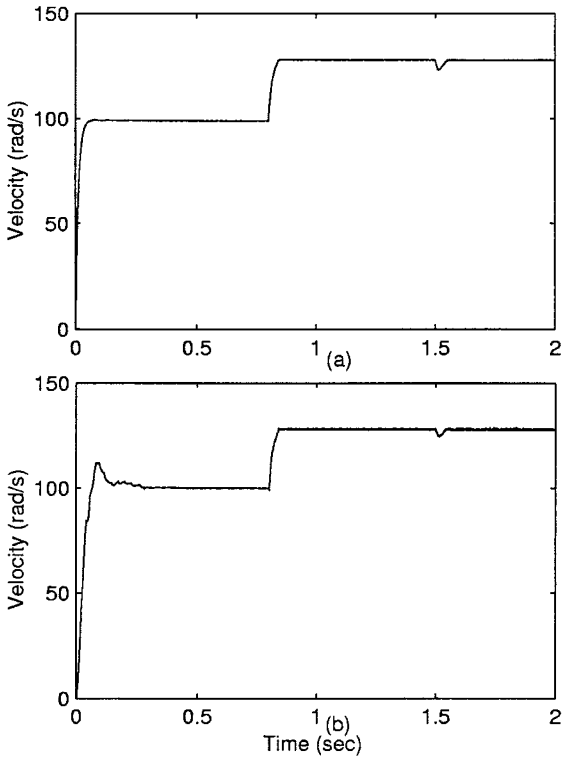

Fig. 17. Simulation of speed responses of the SCHOC under speed and load torque change as in the experiments for different sampling rates: (a) 10 kHz and (b) 8.7 kHz.

execution frequency for the SCHOC in the implemented system (8.7 kHz) was lower than that of the simulation frequency (10 kHz). However, with future faster versions of the dsp board, this problem should be able to be overcome.

In order to verify this assumption, the SCHOC system was resimulated at a lower execution frequency of 8.7 kHz (with the same speed commands and torque as for the above experimental results). The results of this simulation are shown in Fig. 17, where the simulated results comparing 8.7 kHz with 10 kHz are shown. The results are not exactly the same as for the experimental results at 8.7 kHz (due to the above mentioned experimental actual operating effects). However, the general observation that the transient overshoot is poorer for the lower frequency can be verified by the simulation results again.

VIII. Conclusion

As mentioned earlier, in cases where problems could be solved by either soft or hard computing, or both methodologies, an important research question is what are the advantages for fusing SC methods together with HC methods, rather than using the HC method alone. Hence, in this paper, a performance comparison of a fused soft control–hard observer type controller and a hard control–hard observer type controller was given.

Hence, two sensorless speed controllers for the SRM were proposed, namely the HCHOC and the SCHOC. The first type is based on classical hard computing control exclusively where the second is based on the fusion of both hard and soft computing control methodologies. In both the HCHOC and the SCHOC, a reduced order nonlinear observer is adopted to provide position and velocity estimations and thus provide a sensorless system. In the HCHOC, the observer is combined with a robust feedback linearization controller, whilst in the SCHOC, the observer is combined with a adaptive fuzzy controller.

A major aim of the research was to compare rigorously the performance of both the soft computing and classical type controllers under exactly the same condition. Thus, performance comparisons were made for a wide range of operating conditions for SRM. These included startup, step changes in reference speed, unknown load torque, parameters variations, measurement noises, and standstill and stall.

As feedback linearization technique essentially need accurate modeling parameters and position and estimation information, it was found that the HCHOC gives a poor performance under the different SRM operating conditions tested even after a robust term is added.

On the other hand, the SCHOC was found to provide a very satisfactory performance for SRM sensorless speed control. Incorporating a nonlinear SRM model, an observer and adaptive fuzzy control, the SCHOC overcomes the problem associated with the motor complex and nonlinear characteristics and provides a high performance speed controller for SRM under the wide range of operation conditions tested.

Furthermore, the SCHOC also provide a very satisfactory position and speed estimation under the above mentioned operation conditions, thus overcomes the disadvantages of requiring position and speed sensors.

Experimental results, although not as ideal as the simulation results, also confirm the advantage of fused SC and HC control.

Hence, it can be concluded that the fused soft and hard computing type SCHOC offered significant advantages comparing with the classical hard type HCHOC.

APPENDIX
SRM PARAMETERS

$$q = 4.$$
$$N_r = 6.$$
$$r = 1.4\ \Omega.$$
$$P_N = 1\ \text{HP}.$$
$$V_N = 240\ \text{V}.$$
$$I_N = 8.5\ \text{A}.$$
$$a = 0.1360\ 1/\text{A}.$$
$$b = 0.1034\ 1/\text{A}.$$
$$\Omega_N = 4000\ \text{rpm}.$$
$$\psi_s = 0.2886\ \text{Wb}.$$
$$B = 0.002\ \text{Nms/rad}.$$
$$J = 0.0004\ \text{Kg-m}^2.$$

REFERENCES

[1] M. Spong, R. Marino, S. Peresada, and D. G. Taylor, "Feedback linearizing control of a switched reluctance motors," *IEEE Trans. Automat. Contr.*, vol. AC-32, pp. 371–379, May 1987.

[2] G. Buja, R. Menis, and M. Valla, "Variable structure control of an SRM drive," *IEEE Trans. Ind. Electron.*, vol. 40, pp. 56–63, Feb. 1993.

[3] S. Panda, C. Low, and P. K. Dash, "Hybrid feedback linearization-fuzzy controller for variable reluctance motors," *Int. J. Electron.*, vol. 80, no. 2, pp. 155–167, 1996.

[4] S. Mir, M. Elbuluk, and I. Husain, "Torque-ripple minimization in switched reluctance motors using adaptive fuzzy control," *IEEE Trans. Ind. Applicat.*, vol. 35, pp. 461–468, Mar./Apr. 1999.

[5] A. Cheok and N. Ertugrul, "Sensorless rotor position detection techniques in switched reluctance motor drives," in *Proc. Australasian Univ. Power Eng. Conf.*, Perth, Australia, 1995, pp. 84–89.

[6] A. Lumsdaine and J. Lang, "State observers for variable reluctance motors," *IEEE Trans. Ind. Electron.*, vol. 37, pp. 133–142, Apr. 1990.

[7] Y. Zhan, C. Chan, and K. Chau, "A novel sliding-mode observer for indirect position sensing in switched reluctance motor drives," *IEEE Trans. Ind. Electron.*, vol. 46, pp. 390–397, Apr. 1999.

[8] J. Solsona, M. Etchechoury, M. Valla, and C. Muravchik, "Position and speed estimation of a switched reluctance motor," *Int. J. Electron.*, vol. 86, no. 4, pp. 487–507, 1999.

[9] M. Islam and I. Husain, "Torque ripple minimization with indirect position and speed sensing for switched reluctance motors," *IEEE Trans. Ind. Electron.*, vol. 47, pp. 1126–1133, Oct. 2000.

[10] P. J. C. Branco and J. A. Dente, "An experiment in automatic modeling an electrical drive system using fuzzy logic," *IEEE Trans. Syst. Man Cybern. C*, vol. 28, pp. 254–262, May 1998.

[11] G. C. Mouzouris and J. M. Mendel, "Dynamic nonsingleton fuzzy logic systems for nonlinear modeling," *IEEE Trans. Fuzzy Syst.*, vol. 5, no. 2, pp. 199–208, 1997.

[12] J. van den Berg and D. Ettes, "Representation and learning capabilities of additive fuzzy systems," in *Proc. 1998 IEEE Int. Conf. Intelligent Engineering Systems*, 1998, pp. 121–126.

[13] A. Fitzgerald, C. Kinglsey, and S. Umans, *Electric Machinery*. New York: McGraw-Hill, 1983.

[14] T. Miller and G. McGilp, "Nonlinear theory of the switched reluctance motor for rapid computer-aided design," *Proc. Inst. Elect. Eng. B*, vol. 137, pp. 337–347, Nov. 1990.

[15] J. Slotine and W. Li, *Applied Nonlinear Control*. Englewood Cliffs, NJ: Prentice-Hall, 1991.

[16] S. Panda and P. K. Dash, "Application of nonlinear control to switched reluctance motors: a feedback linearization approach," *Proc. Inst. Elect. Eng., Elect. Power Applicat.*, vol. 143, no. 5, pp. 371–379, 1996.

[17] F. Blaabjerg, L. Christensen, S. Hansen, J. Kristoffersn, and P. Rasmussen, "Sensorless control of switched reluctance motor with variable-structure observer," *Electromotion*, vol. 3, pp. 141–152, 1996.

[18] L. Wang and J. Mendel, "Fuzzy basis fuctions, universal approximation, and orthogonal least squares learning," *IEEE Trans. Neural Networks*, vol. 3, pp. 807–814, Sept. 1992.

[19] C. G. Lee and C.-T. Lin, *Neural Fuzzy Systems: A Neuro-Fuzzy Synergism to Intelligent Systems*. Upper Saddle River, NJ: Prentice-Hall, 1996.

[20] S. Sastry and A. Isidori, *Adaptive Control: Stability, Convergence, and Robustness*. Englewood Cliffs, NJ: Prentice-Hall, 1989.

[21] L.-X. Wang, *Adaptive Fuzzy Systems and Control: Design and Stability Analysis*. Upper Saddle River, NJ: Prentice-Hall, 1994.

[22] A. Cheok and N. Ertugrul, "High robustness and reliability of fuzzy logic based position estimation for sensorless switched reluctance motor drives," *IEEE Trans. Power Electron.*, vol. 15, pp. 319–334, Mar. 2000.

Chunming Shi (S'00–M'01) received the B.Eng degree from the Department of Automation, University of Science and Technology of China, in 1999, and the M.Eng degree from the Department of Electrical and Computer Engineering, National University of Singapore, in 2002. His research interests include nonlinear control, signal processing, and soft computing.

Adrian David Cheok (M'92) received the B.Eng (Hons. First) and Ph.D degrees from the University of Adelaide, Australia, in 1993 and 1998 respectively.

From 1996 to 1998, he worked at Mitsubishi Electric Research Labs, Japan. Since 1998, he has been Assistant Professor in the Department of Electrical Engineering, National University of Singapore. His research interests include power electronics and motor drives, fuzzy logic and soft computing, real-time systems, wearable computers, and mixed reality.